Applied Catalysis B: Environmental 174–175 (2015) 496–503

Contents lists available at ScienceDirect

Applied Catalysis B: Environmental

journal homepage: www.elsevier.com/locate/apcatb

Extremely efficient full solar spectrum light driven thermocatalytic activity for the oxidation of VOCs on OMS-2 nanorod catalyst

Mingyang Mao, Yuanzhi Li*, Jingtao Hou, Min Zeng, Xiujian Zhao

State Key Laboratory of Silicate Materials for Architectures (Wuhan University of Technology), 122 Luoshi Road, Wuhan 430070, PR China

ARTICLE INFO

Article history:
Received 24 December 2014
Received in revised form 14 March 2015
Accepted 22 March 2015
Available online 24 March 2015

Keywords:
VOC purification
Full solar spectrum catalysis
OMS-2
Catalytic stability

ABSTRACT

The cryptomelane-type octahedral molecular sieve (OMS-2) nanorod catalysts with different concentration of oxygen vacancy exhibit strong absorption across the full solar spectra. The OMS-2 catalysts can efficiently transform the absorbed solar energy to thermal energy, resulting in a considerable increase of temperature up to 220 °C. By combining the strong absorption across the full solar spectrum and the highly efficient thermocatalytic activity of the OMS-2 catalyst with high concentration of oxygen vacancies, full solar spectrum, visible-infrared, and infrared light driven thermocatalysis with extremely high efficiency are achieved. Under the irradiation of full solar spectrum, visible-infrared, and infrared light, the OMS-2 catalyst exhibits extremely high catalytic activity and excellent durability for the oxidation of organic pollutants such as benzene, toluene, and acetone. Under the full solar spectrum irradiation, the initial CO_2 formation rate of the OMS-2 catalyst for benzene oxidation is 22.1 times larger than that of Bi_2WO_6/TiO_2, a near-infrared photocatalyst reported recently. After the OMS-2 catalyst was recycled for 40 times, its catalytic activity remains unchanged. A novel mechanism of solar light driven thermocatalysis is proposed, and the reason why the OMS-2 catalyst with high concentration of oxygen vacancies exhibits the extremely high catalytic activity is discussed.

1. Introduction

Volatile organic compounds (VOCs) as major air pollutants are not only hazardous to human health but also harmful to the environment. Developing a highly efficient and cost-effective catalyst and strategy for the cleanup of VOCs is highly desirable [1]. Photocatalytic cleanup of VOCs has been regarded as one of most promising technologies. Among the diverse nanostructured photocatalysts, nanostructured TiO_2 has attracted much research attention because of its superior photocatalytic activity, catalytic stability, low cost, and nontoxicity [1–9]. However, it is activated only under UV light irradiation because of its large band gap (3.2 eV for anatase, and 3.0 eV for rutile). Solar spectra contain ~5% ultraviolet (UV) and ~50% visible light (400 ~ 700 nm), and the rest of the solar radiation lies in the infrared part. Therefore, it is extremely crucial and of scientific dream to develop full solar spectrum light driven photocatalysts. To do so, persistent efforts have been devoted to narrowing the band gap of TiO_2 by doping various nonmetals and transition metals [3–9], to synthesizing diverse photocatalysts with narrow band gap [10–16], to preparing visible-light plasmonic photocatalyts [17,18]. Most of these studies were focused on visible photocatalysts, only very few efforts have been made in preparing near-infrared photocatalysts by combining photocatalyst and upconversion materials [19–22], hydrogen-treated WO_3 [23], $Cu_2(OH)PO_4$ [24], and Bi_2WO_6-based hybrid photocatalyst [25]. The band gap narrowing strategies face a dilemma: First, the band gap narrowing via lowering the level of conduction band, or lifting the level of valence band, or both, inevitably causes an implicit conflict between the wide visible or infrared absorption and the adequate redox capability [16]. Second, the band gap narrowing leads to an increase in the number of photons with energy higher than the band gap, resulting in more energy loss through electron–phonon interaction for the excess photon energy. Third, mechanistic studies clearly demonstrate that the majority of photogenerated electrons and holes recombines, resulting in low quantum efficiency [26,27]. Finally, highly efficient near-infrared photocatalysis based on upconversion materials at moderate light intensities is limited by their weak and narrow band near-infrared absorption [28]. Therefore, it is very difficult to achieve high efficiency photocatalysis activated by the full solar spectrum light if the conventional route of band gap narrowing of photocatalytic semiconductors or utilizing upconversion is followed [16,26–28].

* Corresponding author. Tel.: +86 13297971196.
E-mail address: liyuanzhi66@hotmail.com (Y. Li).

http://dx.doi.org/10.1016/j.apcatb.2015.03.044
0926-3373/

OMS-2 is a type of manganese oxide with edge and corner shared MnO_6 octahedra, forming a 2×2 tunnel structure with K^+ ions inside the tunnel for charge balancing. Because of its unique structural characteristics, OMS-2 has been extensively investigated for diverse applications of thermocatalytic oxidation such as chemical synthesis, cleanup of organic pollutants [29–37]. Recently, we developed an approach of hydrothermal redox reaction to prepare OMS-2 nanorods with tunable concentration of oxygen vacancy defects (OVDs). We demonstrated a giant OVD effect on the thermocatalytic activity of OMS-2. Increasing the OVD concentration considerably enhances the lattice oxygen reactivity, thus tremendously promoting the thermocatalytic activity (the reaction temperature of T_{90} (90% conversion decreased by 102 °C) [35]. For the thermocatalysis, thermal source must be provided. It is highly desirable to achieve the catalytic synthesis and environmental cleanup using renewable solar energy. Herein, for the first time, we realize full solar spectrum, visible-infrared, and infrared thermocatalysis with extremely high efficiency for the oxidation of VOCs by developing a conceptually new strategy of solar light driven thermocatalysis, combining light absorption across the full solar spectrum with highly efficient thermocatalytic activity of OMS-2 nanorods.

2. Experimental

2.1. Preparation

OMS-2 nanorod catalysts were prepared by a facile method of hydrothermal reaction between $Mn(NO_3)_2$ (AR,50 wt%), and $KMnO_4$(AR, ≥99.5%) at different temperature dscribed in our previous work [35]. The detailed procedure is as follows. 3.5790 g of $Mn(NO_3)_2$ was dissolved in 40 mL of distilled water in a beaker. 3.1608 g of $KMnO_4$ was rapidly added into the $Mn(NO_3)_2$ aqueous solution under magnetic vigorous stirring until it was dissolved. Then, the mixture solution was transferred to a 100 mL Teflon bottle, and sealed tightly in a stainless-steel autoclave. The autoclave was placed in an electrical oven, heated to 70 °C, and kept at the temperature for 24 h. After the autoclave was cooled to room temperature, the resulting precipitate was washed with distilled water, and dried under an infrared lamp. The obtained sample was denoted as OMS-70. The preparation procedures for OMS-90 and OMS-180 are the same as that for OMS-70 except for heating the autoclave to 90, 180 °C, respectively.

The near-infrared photocatalyst of Bi_2WO_6/TiO_2 was prepared according to the procedure reported by Tian et al. [25].

2.2. Characterization

Diffusive reflectance UV–vis (DRUV–vis) absorption spectra were recorded on a UV-3600 spectrophotometer. The OMS-2 samples were analyzed by a VG Multilab 2000 X-ray photoelectron spectrometer (XPS) using Mg Kα radiation. Their Mn 3s spectra were deconvoluted by using special software. The thermal capacity (C_p) of the samples at different temperature was measured on a C80 micro calorimeter (SETARAM).

2.3. Catalytic activity

The solar light driven thermocatalytic oxidation of organic compounds on the catalysts was tested on a closed cylindrical stainless steel gas-phase reactor (447 mL) with a quartz window (110 mm in diameter). A Xe lamp system (CHF-XM500, Beijing Changtuo Co.) was placed in the front of the quartz window of the reactor. In order to avoid energy loss, 0.1000 g of the catalyst was coated on a thermal insulation slice (4 cm × 4 cm) of aluminum silicate fiber, which was subsequently placed on the bottom of the reactor. A thermocouple was put on the catalyst to measure the temperature under the irradiation of the Xe lamp. To measure the visible-infrared and infrared light driven catalytic activity, a cutoff filter of 420, 480, 560, 690 or 830 nm was placed between the Xe lamp and the quartz window of the reactor to filter out the irradiation with wavelength below 420, 480, 560, 690 or 830 nm from the Xe lamp. The reactor was connected to a GC9560 gas chromatograph (GC) equipped with a flame ionization detector (FID), a methane converter, a Porapak R column and PEG20M column through an automatically sampling ten-way valve (VALCO) with an air actuator by a micropump. The test for the catalytic oxidation of OVCs was carried out in air in the reactor. The oxygen content in the reactor is 20 vol%. Before the catalytic oxidation of organic compounds, the Xe lamp was turned on until the measured concentration of CO_2 remained unchanged to ensure the removal of all adventitious organic compounds adsorbed on the catalyst and the adsorption–desorption equilibrium of CO_2 on the catalyst. Then, a known amount of organic compound (e.g., 2 μL of benzene or toluene, 20 μL of acetone) was injected in the reactor from an injection pore sealed with silicone rubber, and the catalytic oxidation started, resulting in an increase of CO_2 concentration. The adsorption of the VOC reactants on the inner wall of the stainless steel reactor is unavoidable. On the other hand, as air contains a certain amount of CO_2, the adsorption of CO_2 on the inner wall of the reactor and the catalyst is saturated. Therefore, we use the CO_2 formation rate to evaluate the catalytic activity of the catalysts. The concentration of CO_2 produced was obtained by subtracting the initial concentration of CO_2 in the reactor.

The spectral profile of the irradiation of the Xe lamp was recorded on a QM/TM/NIR spectrofluorometer (PTI). The incident light intensity from the Xe lamp was measured by an optical power meter (Newport 1918-R) connected to a thermopile sensor (Newport 818P-001-12) and a UV-365 (320 ~ 400 nm) radiometer. The total intensity of incident light from the Xe lamp (full solar spectrum light) on the catalysts is 301.7 mW cm^{-2}. After filtering out the irradiation with wavelength below 420, 480, 560, or 690 nm, the intensity of incident light from the Xe lamp is 270.4, 248.0, 237.8, 176.3 mW cm^{-2}, respectively [38].

The procedure for the recycled experiments of benzene oxidation on the catalyst under the irradiation of the full solar spectrum light is as follows. After the first cycle of catalytic activity test, the reactor was opened to remove the products (e.g., CO_2) with fresh air and covered again. Then, 2 μL of benzene was injected in the reactor, and the Xe lamp was turned on to start next test of the catalytic oxidation. The reaction time of each cycle is 30 min. The procedure was repeated for known times. The procedure for the recycled experiments of the acetone oxidation is the same as that of benzene oxidation except for injecting 40 μL acetone in each test cycle of 20 min.

3. Resutls and discussion

3.1. Characterization

The OMS-2 nanorod samples with different OVD concentration were prepared by a facile method of hydrothermal redox reaction between $Mn(NO_3)_2$ and $KMnO_4$ at 180, 90, and 70 °C, respectively [35]. The obtained samples, denoted as OMS-180, OMS-90, and OMS-70, were characterized by XRD, TEM, BET, XPS, Raman, etc. [35]. All the samples have cyrstalline structure of pure tetragonal cryptomelane and mophology of nanorods (Fig. S1 and S2). The BET surface area of OMS-180, OMS-90, and OMS-70 is 33.2, 58.2, and 75.8 m^2 g^{-1}, respectively. The Mn^{3+}/Mn^{4+} atomic ratio of OMS-180, OMS-90, and OMS-70, which is determined by analysing their Mn 2p XPS spectra, is 1.0, 2.1, and 3.1, respectively [35].

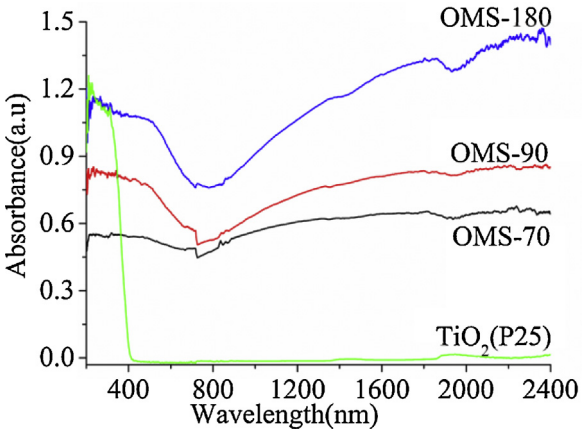

Fig. 1. UV–vis-IR spectra of the samples.

According to the Mn^{3+}/Mn^{4+} atomic ratio, the relative OVD concentration (z, $K_xMn(III)_yMn(IV)_{1-y}O_{2-z}$) in OMS-180, OMS-90, and OMS-70 is calculated to be 0.20, 0.29, and 0.32, respectively. The relative OVD concentration is also determined by the average oxidation state (AOS) of Mn in the OMS-2 samples, which can be calculated by using the magnitude of Mn 3s multiplet splitting (Fig. S3) according to the following formula [37,39]:

$$AOS = 8.95 - 1.13\Delta Es(eV)$$

where ΔEs represents the multiplet spitting, which is the energy difference between the main peak and its satellite. The obtained ΔEs of OMS-180, OMS-90, and OMS-70 is 5.05, 4.95, 4.84 eV, respectively. The calculated AOS decreases in the sequence of OMS-180 (3.48) < OMS-90 (3.36) < OMS-70 (3.24). According to the AOS, the relative OVD concentration in OMS-180, OMS-90, and OMS-70 is calculated to be 0.18, 0.22, and 0.31, respectively, which is in general agreement to the corresponding data by analyzing their Mn 2p XPS.

Fig. 1 shows the absorption spectra of OMS-180, OMS-90, and OMS-70. As shown in Fig. 1, all the OMS-2 samples exhibit strong absorption in whole region of solar spectrum from ~200 nm to ~2400 nm with relatively weak absorption around 780 nm. In striking contrast, TiO_2(P25), a widely used benchmark photocatalyst, only exhibits absorption in UV region. It can be seen from Fig. 1 that the absorption of the OMS-2 nanorod samples can be considerably altered by tuning the OVD concentration of OMS-2. OMS-180 with the lowest OVD concentration exhibits the strongest absorption. Increasing the OVD concentration leads to a considerable decrease of absorbance in the whole region of solar spectrum. OMS-70 with the highest OVD concentration exhibits the lowest absorbance.

3.2. Catalytic activity

3.2.1. Catalytic oxidation of benzene

Benzene is one of priority hazardous VOCs in polluted urban atmosphere for which efficient cleanup technologies are needed. The catalytic activity of the catalysts was investigated by evaluating the rate of CO_2 formation from benzene oxidation under the irradiation of a Xe lamp, which has spectra similar to the solar spectra (Fig. S4). For OMS-180 with the lowest OVD concentration, benzene is oxidized with increasing irradiation time (Fig. 2A). The reaction products contained only CO_2 and H_2O, and no other byproducts were detected by the gas chromatograph for the OMS-2 catalysts. The concentration of CO_2 produced is 4631.7 mg m^{-3} after the full solar spectrum irradiation for 30 min (Fig. 2B). Increasing the OVD concentration in the OMS-2 nanorod samples leads to a significant increase of catalytic activity. Compared to OMS-180, OMS-90 with

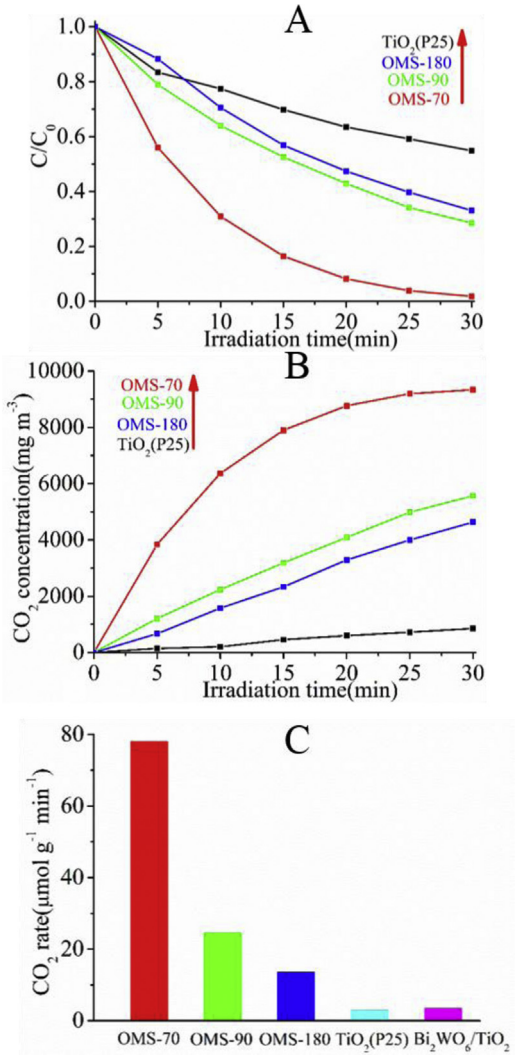

Fig. 2. Time course of benzene concentration (A), CO_2 concentration (B), r_{CO_2} (C) for benzene oxidation on the catalysts).

higher OVD concentration shows higher catalytic activity. Its concentration of CO_2 produced increases to 5570.6 mg m^{-3} after the full solar spectrum irradiation for 30 min. OMS-70 with the highest OVD concentration exhibits the highest catalytic activity, its concentration of CO_2 produced increases to 9337.1 mg m^{-3} after the full solar spectrum irradiation for 30 min. Fig. 2C compared the initial CO_2 production rate in first 5 min (r_{CO_2}) for the OMS-2 nanorod catalysts. r_{CO_2} of OMS-70 (78.06 μmol $g^{-1}_{\text{-catal}}$ min^{-1}) is 3.2 and 5.7 times higher than that of OMS-90 and OMS-180, respectively. As the OMS-2 catalysts have different specific surface areas, we compared their specific CO_2 formation rate (per unit surface area of catalyst), which represents the specific catalytic efficiency of the OMS-2 catalysts. The specific CO_2 formation rate of OMS-70 (1.03 μmol $m^{-2}_{\text{-catal}}$ min^{-1}) is 2.4 and 2.5 times larger than that of OMS-90 (0.42 μmol $g^{-1}_{\text{-catal}}$ min^{-1}) and OMS-180 (0.41 μmol $g^{-1}_{\text{-catal}}$ min^{-1}), respectively. For comparison, we tested the photocatalytic activity of TiO_2(P25), widely used as benchmark photocatalyst, for benzene oxidation under the full solar spectrum irradiation. After the full solar spectrum irradiation for 30 min, the concentration of CO_2 produced is only 855.1 mg m^{-3}. Its r_{CO_2} (2.94 μmol $g^{-1}_{\text{-catal}}$ min^{-1}) is 26.5 times lower than that of OMS-70. Recently, Tian et al. reported a near-infrared photocatalyst of Bi_2WO_6/TiO_2 for the liquid-phase photodegradation of dye such as methyl orange [25]. For comparison, we also tested

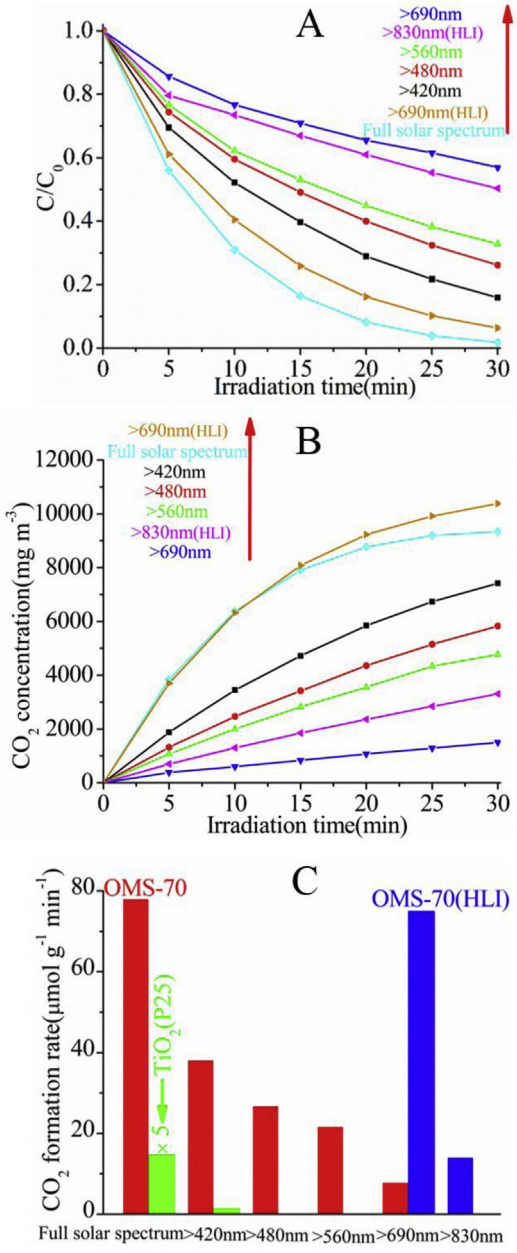

Fig. 3. Time course of benzene concentration (A), CO_2 concentration (B), and r_{CO_2} (C) for benzene oxidation on OMS-70 and TiO_2(P25) under the full solar spectrum irradiation, visible-infrared irradiation, and infrared irradiation by using different cut-off filters, and on OMS-70 under the irradiation of high light intensity (HLI, blue). (For interpretation of the references to color in this figure legend, the reader is referred to the web version of this article.)

the photocatalytic activity of Bi_2WO_6/TiO_2 for the gas-phase photodegradation of benzene under the full solar spectrum irradiation. After the full solar spectrum irradiation for 20 min, the CO_2 concentration of Bi_2WO_6/TiO_2 is only 684.6 mg m^{-3}. r_{CO_2} of Bi_2WO_6/TiO_2 (3.52 μmol $g^{-1}_{\text{-catal}}$ min^{-1}) is 22.1 times lower than that of OMS-70 (Fig. 2C). These results indicate that OMS-2 exhibits highly efficient catalytic activity under the full solar spectrum irradiation and its catalytic activity can be significantly improved by increasing the OVD concentration of OMS-2.

We tested the catalytic activity of the catalysts for benzene oxidation under the visible-infrared and infrared irradiation of the Xe lamp by using different cutoff filters. As shown in Fig. 3A, benzene is quickly oxidized on OMS-70 under the visible-infrared irradiation above 420 nm. After the visible-infrared irradiation above 420 nm for 30 min, the concentration of CO_2 produced is 7417.7 mg m^{-3} (Fig. 3B). r_{CO_2} of OMS-70 is as high as 38.16 μmol $g^{-1}_{\text{-catal}}$ min^{-1} (Fig. 3C). In contrast, r_{CO_2} of TiO_2 (P25) is only 0.29 μmol $g^{-1}_{\text{-catal}}$ min^{-1}, which is 131.6 times lower than that of OMS-70.

Under the visible-infrared irradiation above 480 nm, benzene is still quickly oxidized to CO_2 on OMS-70. After the visible-infrared irradiation above 480 nm for 30 min, the concentration of CO_2 produced is 5826.3 mg m^{-3}. r_{CO_2} of OMS-70 is as high as 26.78 μmol $g^{-1}_{\text{-catal}}$ min^{-1}. However, benzene cannot be oxidized without detectable CO_2 produced under the visible-infrared irradiation above 480 nm for TiO_2 (P25), which is attributed to that TiO_2 cannot be excited by visible light due to its large band gap.

We further tested the catalytic activity of OMS-70 for benzene oxidation under the visible-infrared irradiation above 560 nm and 690 nm. In both cases, OMS-70 still exhibit efficient catalytic activity. After the visible-infrared irradiation above 560 nm for 30 min, the concentration of CO_2 produced is 4765.7 mg m^{-3}. r_{CO_2} of OMS-70 is 21.7 μmol $g^{-1}_{\text{-catal}}$ min^{-1}. Remarkably, even under the visible-infrared irradiation above 690 nm, benzene is still efficiently oxidized to CO_2 on OMS-70.

Compared to the catalytic activity of OMS-70 under the full solar spectrum irradiation, the catalytic activity significantly decreases under the visible-infrared irradiation above 690 nm (Fig. 3C). This is due to a considerable decrease of the irradiation energy from 301.7 to 176.3 mW cm^{-2}. To confirm this explanation, we increased the light intensity of the visible-infrared irradiation above 690 nm from 176.3 to 391.0 mW cm^{-2} by decreasing the distance between the Xe Lamp and the reactor. As shown in Fig. 3C, under the higher light intensity (HLI) of the visible-infrared irradiation above 690 nm, r_{CO_2} of OMS-70 significantly increases from 7.84 to 74.93 μmol $g^{-1}_{\text{-catal}}$ min^{-1}. We also tested the catalytic activity of OMS-70 for benzene oxidation under the higher light intensity (HLI) of the infrared irradiation above 830 nm (315.2 mW cm^{-2}). In this case, benzene is still efficiently oxidized to CO_2 on OMS-70, and r_{CO_2} of OMS-70 is 14.11 μmol $g^{-1}_{\text{-catal}}$ min^{-1}.

3.2.2. *Catalytic oxidation of toluene and acetone*

We tested the catalytic activity of OMS-70 and TiO_2 (P25) under the full solar spectrum irradiation and the visible-infrared irradiation for the oxidation of other VOCs such as toluene and acetone. For toluene oxidation, OMS-70 exhibits highly efficient photocatalytic activity under the full solar spectrum irradiation and the visible-infrared irradiation (Fig. 4). Under the full solar spectrum irradiation, toluene is very quickly oxidized to CO_2. Its r_{CO_2} of OMS-70 (99.14 μmol $g^{-1}_{\text{-catal}}$ min^{-1}) is 33.1 times larger than that of TiO_2 (P25). Under the visible-infrared irradiation above 420 nm, r_{CO_2} of OMS-70 is very high (74.95 μmol $g^{-1}_{\text{-catal}}$ min^{-1}), which is 189.3 times higher than that of TiO_2(P25). Under the visible-infrared irradiation above 480 and 560 nm, OMS-70 still exhibits efficient catalytic activity, its r_{CO_2} is as high as 53.47, 30.19 μmol $g^{-1}_{\text{-catal}}$ min^{-1}, respectively. In contrast, under the visible-infrared irradiation above 480 nm, TiO_2 (P25) has no photocatalytic activity for toluene oxidation. Remarkably, even under the visible-infrared irradiation above 690 nm, toluene can be efficiently oxidized to CO_2 on OMS-70, although its r_{CO_2} decreases to 8.35 μmol $g^{-1}_{\text{-catal}}$ min^{-1}.

For acetone oxidation, OMS-70 exhibits extremely high efficiency under the full solar spectrum irradiation (Fig. 5). Its r_{CO_2} (999.60 μmol $g^{-1}_{\text{-catal}}$ min^{-1}) is much higher than that for the catalytic oxidization of both benzene and toluene. This is because the oxidation of acetone with lower oxidation potential is easier than that of both benzene and toluene with higher oxidation potential [40]. r_{CO_2} of OMS-70 is 36.2 times higher than that of TiO_2(P25) (27.59 μmol $g^{-1}_{\text{-catal}}$ min^{-1}). Under the visible-infrared irradiation above 420, 480, and 560 nm, r_{CO_2} of OMS-70 slightly decreases

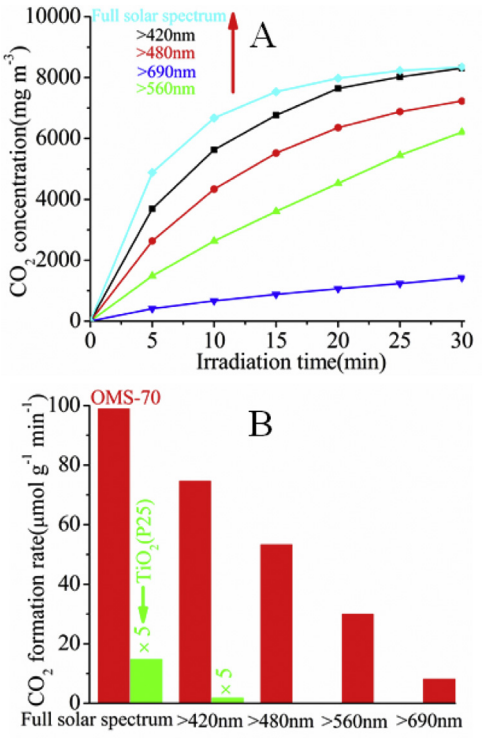

Fig. 4. Time course of CO_2 produced (A) and r_{CO_2} (B) for toluene oxidation on OMS-70 and TiO_2(P25) under the full solar spectrum irradiation and the visible-infrared irradiation by using different cut-off filters.

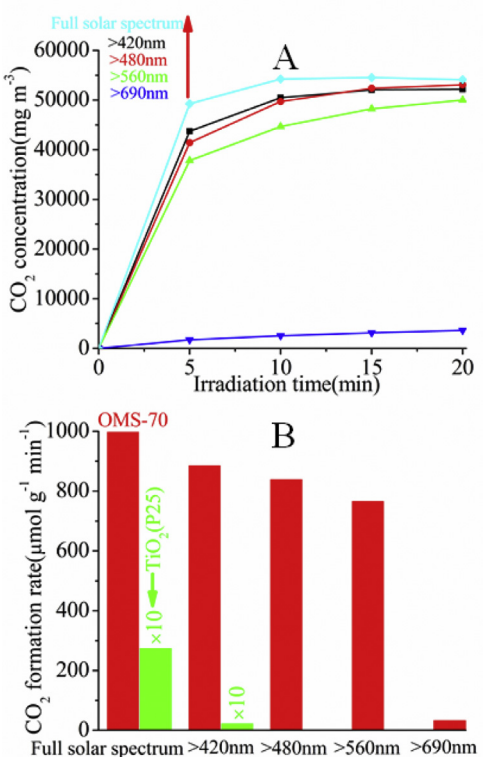

Fig. 5. Time course of CO_2 produced (A) and r_{CO_2} (B) for acetone oxidation on OMS-70 and TiO_2(P25) under the full solar spectrum irradiation and the visible-infrared irradiation by using different cut-off filters.

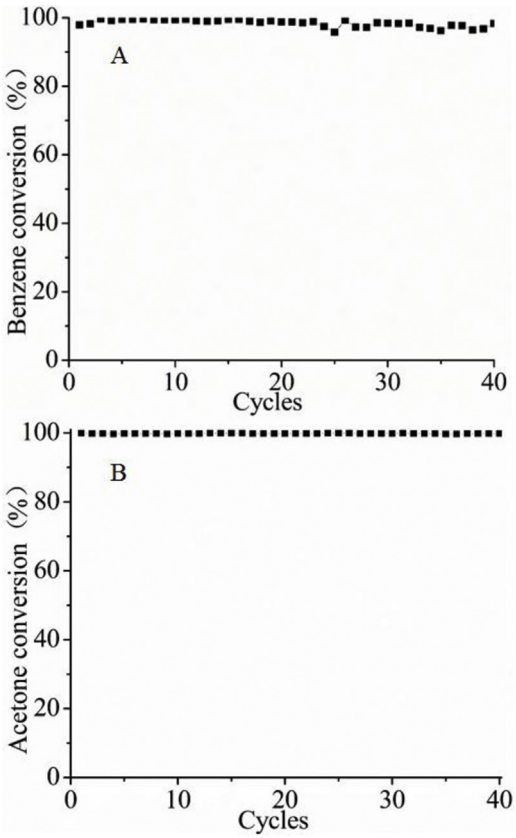

Fig. 6. The stability of OMS-70 for the oxidation of benzene (A) or acetone (B) under the irradiation of the Xe lamp.

to 887.27, 840.67, 767.99 $\mu mol\, g^{-1}_{\text{-catal}}\, min^{-1}$. Even under the visible-infrared irradiation above 690 nm, r_{CO_2} of OMS-70 is as high as 35.05 $\mu mol\, g^{-1}_{\text{-catal}}\, min^{-1}$.

3.2.3. Durability

The catalytic durability of OMS-70 under the full solar spectrum irradiation for benzene oxidation was tested. As shown in Fig. 6A, after the OMS-70 catalyst was recycled for 40 times, its catalytic activity remains unchanged. The catalytic durability of OMS-70 under the full solar spectrum irradiation for acetone oxidation was also tested. As shown in Fig. 6B, after the OMS-70 catalyst was recycled for 40 times, its catalytic activity remains unchanged. The results clearly indicate that the oxidation of VOCs (e.g., benzene and acetone) on OMS-70 is a catalytic process. After the catalytic durability test of OMS-70 for acetone oxidation, the used catalyst of OMS-70 was scratched from the thermal insulation slice and characterized by XRD (Fig. S1) and TEM (Fig. S2). The OMS-2 structure and nanorod morphology of the used OMS-70 almost remained unchanged. These results indicate that OMS-70 shows a good catalytic stability.

3.3. Mechanism

The question is why the OMS-2 catalysts exhibit efficient catalytic activity under the full solar spectrum, visible-infrared, and infrared irradiation. The catalytic activity of the OMS-2 catalysts under the irradiation of the full solar spectrum light maybe arise from the two aspects as follows: one is the well-known photocatalysis [2]. Another is the solar light driven thermocatalysis as the OMS-2 catalysts exhibit efficient thermocatalytic activity [35] and strong absorption in the whole region of solar spectra (Fig. 1).

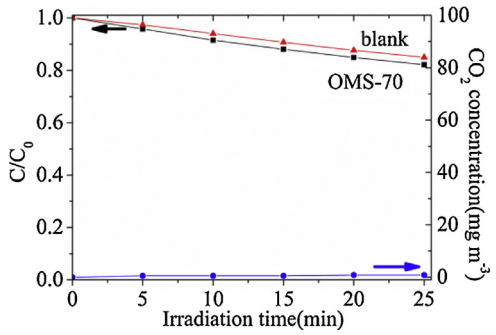

Fig. 7. Time course of benzene and CO_2 produced for the photocatalytic oxidation of benzene on OMS-70 at near room temperature under the irradiation of the Xe lamp (red triangle represents blank test without catalyst). (For interpretation of the references to color in this figure legend, the reader is referred to the web version of this article.)

To confirm whether the former is true, the photocatalytic activity of OMS-70 for benzene oxidation at near room temperature was measured. To do so, 0.1000 g of OMS-70 was coated on a glass slide (4 cm × 4 cm) instead of a thermal insulation slice, which was subsequently placed on the bottom of the reactor with quartz window. The reactor was put in an ice-water bath to maintain the photocatalytic reaction temperature at near room temperature (~40 °C) under the irradiation of the Xe lamp. However, in this case, no benzene is oxidized on OMS-70 without detectable CO_2 produced (Fig. 7), indicating that benzene oxidation on OMS-70 does not take place via the conventional photocatalytic route.

This result suggests that the efficient catalytic activity of the OMS-2 catalysts under the irradiation of the full solar spectrum arises from the solar light driven thermocatalysis as schematically illustrated in Scheme 1: the strong absorption of full solar spectrum light results in a considerable increase of temperature for the OMS-2 catalysts. When the temperature reaches to the light-off temperature of thermocatalytic oxidation on the OMS-2 catalysts, the thermocatalytic reaction starts. The thermocatalytic oxidation on OMS-2 proceeds via the well-known Mars–van Krevelen mechanism [34–37]: organic molecules adsorbed on catalyst surface are oxidized by lattice oxygen, and the resultant oxygen vacancies are subsequently replenished by gas-phase O_2. The lattice oxygen activity of OMS-2 plays a decisive role in the thermocatalytic activity as the reoxidation of reduced OMS-2 is much faster than the reduction of OMS-2 [35,36].

To further confirm the proposed mechanism, we measured the temperature evolution of the OMS-2 catalysts under the irradiation of the Xe lamp (Fig. 8). When the temperature reaches a plateau, equilibrium between the absorption of light energy and the energy dissipation from the catalyst to the surrounding environment is established. The equilibrium temperature at the stage of the plateau in Fig. 8 is defined as plateau temperature. The plateau temperature of OMS-70, OMS-90, and OMS-180 is 220, 209, and 209 °C, respectively. This result suggests that the OMS-2 catalysts can efficiently transform the full solar spectrum light energy to thermal energy, resulting in an increase of temperature for the OMS-2 catalysts. This is because the OMS-2 catalysts have strong absorption in the whole region of solar spectrum from ~200 nm to ~2400 nm (Fig. 1). We measured the photothermal conversion efficiency, which is defined as:

$$\eta = \frac{E_{\text{thermal}}}{E_{\text{phototons}}} \times 100\%$$

$E_{\text{phototons}}$ is the energy of the incident photons, and E_{thermal} is the thermal energy converted by the absorption of the irradiation from the Xe lamp by the catalyst.

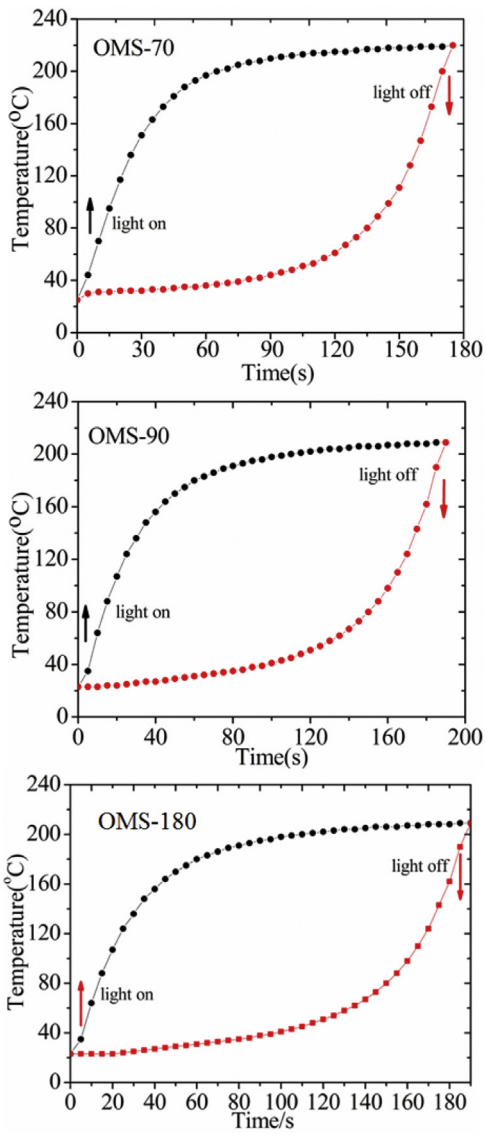

Fig. 8. Temporal change of the temperature on the catalysts under the irradiation of the Xe lamp and after switching off the Xe lamp when temperature reached a plateau.

The photothermal conversion efficiency of OMS-70, OMS-90, and OMS-180 is calculated to be 12.7%, 12.4%, 10.6%, respectively (Fig. S7). The result indicates that OMS-70 and OMS-90 have higher photothermal conversion efficiency than OMS-180. However, the light absorption test shows that OMS-180 has higher absorbance than OMS-90 and OMS-70 (Fig. 1). The possible reason is as follows: the efficiency of photothermal conversion depends on the absorbance of solar light as well as the surface area of absorbing solar light for the catalysts. The higher the absorbance and surface area are, the higher the total solar light energy absorbed is, resulting in the higher plateau temperature. As OMS-70 has higher surface area (75.8 $m^2 g^{-1}$) than OMS-90 (58.2 $m^2 g^{-1}$) and OMS-180 (33.2 $m^2 g^{-1}$), the total solar light energy absorbed for OMS-70 is larger than OMS-90 and OMS-180 (Fig. 1), thus resulting in its higher plateau temperature (Fig. 8). The plateau temperature of OMS-70 and OMS-90 is considerably larger than their corresponding light-off temperature at which the catalytic reaction starts, while the plateau temperature of OMS-180 is slightly larger than its light-off temperature (Fig. S5) [35]. Thus, the solar light driven

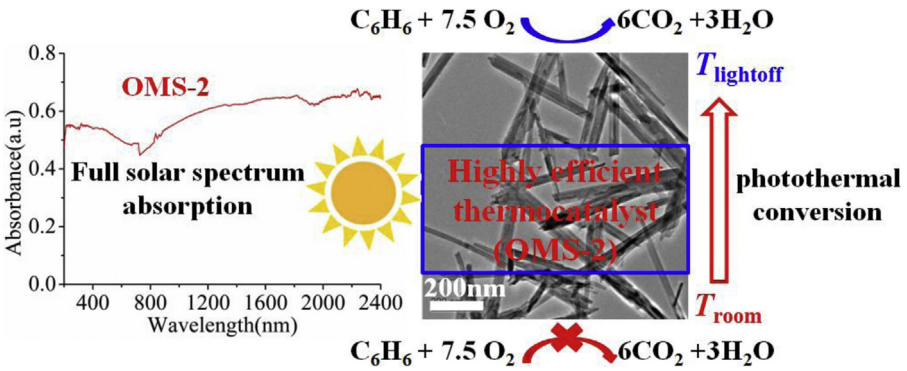

Scheme 1. Schematic illustration of solar light driven themocatalysis.

thermocatalyis for benzene oxidation on the OMS-2 catalyst can take place.

According to the mechanism of solar light driven thermocatalysis, the catalytic activity of the OMS-2 catalysts under the irradiation of the Xe lamp is determined by two factors: (1) the efficiency of photothermal conversion that results in the increase of its temperature, (2) the thermocatalytic activity. OMS-70 has higher photothermal conversion efficiency, evidenced by its higher plateau temperature (220 °C, Fig. 8) than OMS-90 (209 °C) and OMS-180 (209 °C) under the irradiation of the Xe lamp in spite of its lower absorbance (Fig. 1). Meanwhile, OMS-70 with the highest OVD concentration exhibits the highest thermocatalytic activity (Fig. S4) as compared to OMS-90 and OMS-180 due to the OVD effect on the thermocatalytic activity of OMS-2 [35]. The highest thermocatalytic activity of OMS-70 together with its higher efficiency of photothermal conversion results in its highest catalytic activity under the irradiation of the Xe lamp (Fig. 2). Both the lowest thermocatalytic activity of OMS-180 (Fig. S4) and its lower efficiency of photothermal conversion (Fig. 8) lead to its lowest catalytic activity under the irradiation of the Xe lamp (Fig. 2).

We further measured the plateau temperature of OMS-70 under the visible-infrared irradiation of the Xe lamp (Fig. S5). Under the visible-infrared irradiation above 420, 480, 560, and 690 nm, the plateau temperature of OMS-70 is 201, 189, 183, and 157 °C, respectively. This result suggests that OMS-70 could efficiently transform the visible and infrared energy to thermal energy. All the plateau temperatures of OMS-70 under the visible-infrared irradiation above 420, 480, 560, and 690 nm are larger than the light-off temperature for benzene oxidation on OMS-70 (Fig. S5) [35]. This is why OMS-70 exhibits the highly efficient catalytic activity for the oxidation of VOCs such as benzene, toluene, and acetone under the visible-infrared irradiation.

According to the novel mechanism of solar light driven thermocatalysis, two requirements for a catalyst must be satisfied at the same time to realize the full solar spectrum photocatalysis: firstly, the catalyst must exhibit strong absorption in the whole region of solar spectra, and efficiently transfer the absorbed solar energy to thermal energy, resulting in a considerable increase of temperature above the light-off temperature of thermocatalytic reaction. Secondly, the catalyst must exhibit highly efficient thermocatalytic activity with low light-off temperature. It is great challenging to design such catalyst. For example, nano CeO_2 is one of efficient thermocatalyts, and recent works report that nano CeO_2 and Y-doped CeO_2 nanorods exhibit efficient photothermocatalytic activity for the oxidation of organic pollutants [41,42]. However, nano CeO_2 only has strong absorption in the UV–visible region below ~500 nm [41,42]. It is impossible to achieve full solar spectrum light driven catalysis on nano CeO_2. On the other hand, OMS-2 with high crystallinity (e.g., OMS-180) has strong absorption in the whole solar spectrum region (Fig. 1). However, its thermocatalytic activity must be significantly enhanced (Fig. S5). Remarkably, the OMS-2 nanorods with high OVD concentration (OMS-70) can satisfy the two requirements, thus exhibiting full solar spectrum, visible-infrared, and infrared catalytic activity with extremely high efficiency for the oxidation of VOCs such as benzene, toluene, and acetone.

4. Conclusion

In summary, we developed a conceptually new strategy of solar light driven thermocatalysis by combining light absorption across the full solar spectra and highly efficient thermocatalytic activity of the OMS-2 catalyst with high OVD concentration. By this strategy, we realize the full solar spectrum, visible-infrared, infrared light driven thermocatalysis with extremely high efficiency on the OMS-2 catalyst with high OVD concentration for the oxidation of VOCs such as benzene, toluene, and acetone. For the conventional thermocatalysis, thermal source (e.g., electric tube furnace) must be provided to increase temperature. The present solar light driven thermocatalysis provides an energy-saving strategy for the environmental cleanup using renewable solar energy. The strategy have promising applications in solar driven environmental cleanup, catalytic synthesis of chemicals and fuels, and optothermal devices, etc.

Acknowledgements

This work was supported by National Natural Science Foundation of China (21473127, 21273169), Research and Development Project of Hubei Province (2013BAA045), and National Basic Research Program of China (2009CB939704).

Appendix A. Supplementary data

Supplementary data associated with this article can be found, in the online version, at http://dx.doi.org/10.1016/j.apcatb.2015.03.044.

References

[1] H.J. Huang, D.Z. Li, Q. Lin, W.J. Zhang, Y. Shao, Y.B. Chen, M. Sun, X.Z. Fu, Environ. Sci. Technol. 43 (2009) 4164.
[2] X.B. Chen, S.S. Mao, Chem. Rev. 107 (2007) 2891.
[3] S.U.M. Khan, M. Al-Shahry, W.B. Ingler Jr., Science 297 (2002) 2243.
[4] R. Asahi, T. Morikawa, T. Ohwaki, K. Aoki, Y. Taga, Science 293 (2001) 269.
[5] A. Kubacka, M. Fernandez-García, G. Colon, Chem. Rev. 112 (2012) 1555.
[6] X.B. Chen, C. Burda, J. Am. Chem. Soc. 130 (2008) 5018.
[7] S. Livraghi, M.C. Paganini, E. Giamello, A. Selloni, C.D. Valentin, G. Pacchioni, J. Am. Chem. Soc. 128 (2006) 15666.
[8] W. Zhao, W. Ma, C. Chen, J.C. Zhao, Z. Shuai, J. Am. Chem. Soc. 126 (2004) 4782.
[9] H. Kisch, L. Zang, C. Lange, W.F. Maier, C. Antonius, D. Meissner, Angew. Chem. Int. Ed. 37 (1998) 3034.

[10] X.C. Wang, K. Maeda, A. Thomas, K. Takanabe, G. Xin, J.M. Carlsson, K. Domen, M. Antonietti, Nat. Mater. 8 (2009) 76.
[11] M. Higashi, K. Domen, R. Abe, J. Am. Chem. Soc. 134 (2012) 6968.
[12] F. Amano, A. Yamakata, K. Nogami, M. Osawa, B. Ohtani, J. Am. Chem. Soc. 130 (2008) 17650.
[13] L.Z. Zhang, I. Djerdj, M. Cao, M. Antonietti, M. Niederberger, Adv. Mater. 19 (2007) 2083.
[14] J.L. Wang, Y. Yu, L.Z. Zhang, Appl. Catal. B 136 (2013) 112.
[15] L.W. Zhang, Y. Man, Y.F. Zhu, ACS Catal. 1 (2011) 841.
[16] S.X. Ouyang, J.H. Ye, J. Am. Chem. Soc. 133 (2011) 7757.
[17] P. Wang, B.B. Huang, X. Qin, X. Zhang, Y.J. Dai Wei, M.H. Whangbo, Angew. Chem. Int. Ed. 47 (2008) 7931.
[18] C. Hu, T.W. Peng, X.X. Hu, Y.L. Nie, X.F. Zhou, J.H. Qu, H. He, J. Am. Chem. Soc. 132 (2010) 857.
[19] W. Qin, D. Zhang, D. Zhao, L. Wang, K. Zheng, Chem. Commun. 46 (2010) 2304.
[20] S.Q. Huang, L. Gu, C. Miao, Z.Y. Lou, N.W. Zhu, H.P. Yuan, A.S. Shan, J. Mater. Chem. A 1 (2013) 7874.
[21] X.Y. Wu, S. Yin, Q. Dong, B. Liu, Y.H. Wang, T.H. Sekino, S.W. Lee, T. Sato, Sci. Rep. 3 (2013) 2918.
[22] S. Obregon, G. Colon, Chem. Commun. 48 (2012) 7865.
[23] J. Li, Y. Liu, Z.J. Zhu, G.Z. Zhang, T. Zou, Z.J. Zou, S.P. Zhang, D.W. Zeng, C.S. Xie, Sci. Rep. 3 (2013) 2409.
[24] G. Wang, B.B. Huang, X.C. Ma, Z.Y. Wang, X.Y. Qin, X.Y. Zhang, Y. Dai, M.H. Whangbo, Angew. Chem. Int. Ed. 52 (2013) 4910.
[25] J. Tian, Y.H. Sang, G.W. Yu, H.D. Jiang, X.N. Mu, H. Liu, Adv. Mater. 25 (2013) 5075.
[26] J.W. Tang, J.R. Durrant, D.R. Klug, J. Am. Chem. Soc. 130 (2008) 13885.
[27] M. Kong, Y.Z. Li, X. Chen, T.T. Tian, P.F. Fang, F. Zheng, X.J. Zhao, J. Am. Chem. Soc. 133 (2011) 16414.
[28] W. Zou, C. Visser, J.A. Maduro, M.S. Pshenichnikov, J.C. Hummelen, Nat. Photonics 6 (2012) 560.
[29] S.L. Suib, Acc. Chem. Res. 41 (2008) 479.
[30] S. Dharmarathna, C.K. Kingondu, W. Pedrick, L. Pahalagedara, S.L. Suib, Chem. Mater. 24 (2012) 705.
[31] R.H. Wang, J.H. Li, Environ. Sci. Technol. 44 (2010) 4282.
[32] M.A. Peluso, L.A. Gambaro, E. Pronsato, D. Gazzoli, H.J. Thomas, J.E. Sambeth, Catal. Today 133–135 (2008) 487.
[33] W.X. Tang, X.F. Wu, D.Y. Li, Z. Wang, G. Liu, H.D. Liu, Y.F. Chen, J. Mater. Chem. A 2 (2014) 2544.
[34] V.P. Santos, M.F.R. Pereira, J.J.M. Orfao, J.L. Figueiredo, Appl. Catal. B 99 (2010) 353.
[35] J.T. Hou, Y.Z. Li, L.L. Liu, L. Ren, X.J. Zhao, J. Mater. Chem. A 1 (2013) 6736.
[36] J.T. Hou, L.L. Liu, Y.Z. Li, M.Y. Mao, H.Q. Lv, X.J. Zhao, Environ. Sci. Technol. 47 (2013) 13730.
[37] V.P. Santos, O.S.G.P. Soares, J.J.W. Bakker, M.F.R. Pereira, J.J.M. Orfao, J. Gascon, F. Kapteijn, J.L. Figueiredo, J. Catal. 293 (2012) 165.
[38] J.T. Hou, Y.Z. Li, M.Y. Mao, Y.Z. Yue, G.N. Greaves, X.J. Zhao, Nanoscale 7 (2015) 2633.
[39] J.T. Hou, Y.Z. Li, M.Y. Mao, L. Ren, X.J. Zhao, ACS Appl. Mater. Interfaces 6 (2014) 14981.
[40] L. Luo, Y.Z. Li, J.T. Hou, Y. Yang, Appl. Surf. Sci. 319 (2014) 332.
[41] Y.Z. Li, Q. Sun, M. Kong, W.Q. Shi, J.C. Huang, J.W. Tang, X.J. Zhao, J. Phys. Chem. C 115 (2011) 14050.
[42] A.D. Liyanage, S.D. Perera, K. Tan, Y. Chabal, K.J. Balkus Jr, ACS Catal. 4 (2014) 577.